Optical Transmittance of Indium Tin Oxide Nanoparticles Prepared by Laser-Induced Fragmentation in Water

Hiroyuki Usui, Takeshi Sasaki,* and Naoto Koshizaki

Nanoarchitectonics Research Center, National Institute of Advanced Industrial Science and Technology, Central 5, 1-1-1 Higashi, Tsukuba, Ibaraki 305-8565, Japan

Received: March 25, 2006; In Final Form: May 10, 2006

Laser-induced fragmentation of indium tin oxide nanoparticles was performed in water by laser irradiation with various laser energies. Fragmentation of the nanoparticles proceeded with increased laser energy. The fragmented nanoparticles showed high transmittance in the visible region and lower transmittance in the ultraviolet and infrared regions. The optical band gap of the fragmented nanoparticles increased with decreasing average particle size. The increase of the band gap was possibly caused by the Burstein−Moss effect due to the increasing concentration of carriers generated by the surface defects of the oxygen vacancies on smaller nanoparticles.

1. Introduction

Laser ablation of a metal target in solution is a novel and versatile method for preparing various nanomaterials.[1−6] The advantage of this method is the strong confinement of the expanding plasma produced by laser ablation of a target in solution, which can realize extremely high temperature and high pressure.[7] As an additional advantage, the surface modification of obtained nanoparticles and preparation of organic/inorganic composite materials are easily accomplished with the use of a surfactant solution in one simple step.[8,9] Moreover, the surfactant molecules in the solution can prevent particle size increase by their adsorption on the nanoparticles. However, the smallest average size of the obtained nanoparticles is 12 nm, even under an optimal concentration of a suitable surfactant solution in the case of ZnO.[8] Laser-induced fragmentation of nanoparticles dispersed in solution has been recently studied as a method of preparing much smaller nanoparticles.[2,3,10,11] Mafuné et al. obtained gold and platinum nanoparticles of extremely small size (∼1.5 nm) by laser irradiation of source nanoparticles dispersed in solution. However, few reports are available about the preparation of metal oxide and metal alloy nanoparticles using this method.[10] Here we report on an extension of this method to metal oxide nanoparticles.

Indium tin oxide (ITO) is widely used as a transparent conductor due to its high electric conductivity and its good transparency in the visible range. Indium tin oxide nanoparticles are expected to be applied as transparent coating materials for UV and IR shields. Smaller particle size and excellent UV absorption and IR reflection are required in this application. The preparation of 5−30 nm ITO nanoparticles using a wet-chemical method has been already reported.[12−14] However, research on preparation using a physical method is still quite sparse. If much smaller ITO nanoparticles can be produced by laser irradiation of raw ITO nanoparticles in water, then high-quality ITO nanoparticles with less contamination can be generated by a simple one-step method without a chemical reagent. In this study, ITO nanoparticles were irradiated in water by a focused pulsed laser beam to fabricate much smaller ITO nanoparticles, and the particle sizes and the transmittance spectra of the irradiated nanoparticles were investigated to correlate how changes in particle size affect the optical properties of ITO nanoparticles. The mechanisms of particle fragmentation were also analyzed.

2. Experimental Section

The experimental setup for laser irradiation in water is depicted in Figure 1a. Laser irradiation of raw ITO nanoparticles (NanoTek, Sn/In = 1:9, average size = 30 nm) was performed in deionized water for 60 min. Raw ITO nanoparticles (0.8 mg) were dispersed in 40 mL of water, which corresponded to a molar concentration of 7.2×10^{-5} mol/L. A pulsed Nd:YAG laser (Spectra-Physics, LAB-150-10) operating at 10 Hz with a wavelength of 355 nm and a pulse width of 7 ns irradiated the colloidal solution in a glass vial. The laser beam was focused onto the solution by an optical quartz lens with a focal distance of 50 mm. The laser energy was set to 20, 50, 100, and 150 mJ/pulse. A magnetic stirrer was used to prevent gravitational settling of the raw nanoparticles. The zeta potential and secondary particle size of the nanoparticles in the colloidal solutions were measured by electrophoresis and dynamic light-scattering with a particle size analyzer (Malvern, Zetasizer Nano-ZS, 532 nm). The optical transmittances in the UV−vis region of the colloidal solutions were recorded by a UV−vis spectrophotometer (Shimadzu, UV-2100PC). The colloidal solutions were concentrated to 20 times higher concentration by ultracentrifuge and decantation. The 0.5 mL concentrated solutions were dropped and dried in a circle area with a diameter of 8 mm on quartz substrates after ultrasonic agitation for uniform coverage on the substrates. X-ray diffraction (XRD) measurements using an X-ray diffractometer (Rigaku, RAD-C, Cu Kα irradiation) were performed for the dried precipitates on quartz substrates. The diffuse reflectance of the raw ITO nanoparticles and the optical transmittance of UV−vis−IR of the precipitated films were measured by a UV−vis−IR spectrophotometer (Varian, Cary 5000). The solutions before the concentration were dropped on a copper mesh with an amorphous carbon film for observation by a field emission scanning electron microscope

* Author to whom correspondence should be addressed. Phone: +81-29-861-4896. Fax: +81-29-861-6355. E-mail: takeshi.sasaki@aist.go.jp.

10.1021/jp061866f CCC: $33.50
Published on Web 06/13/2006

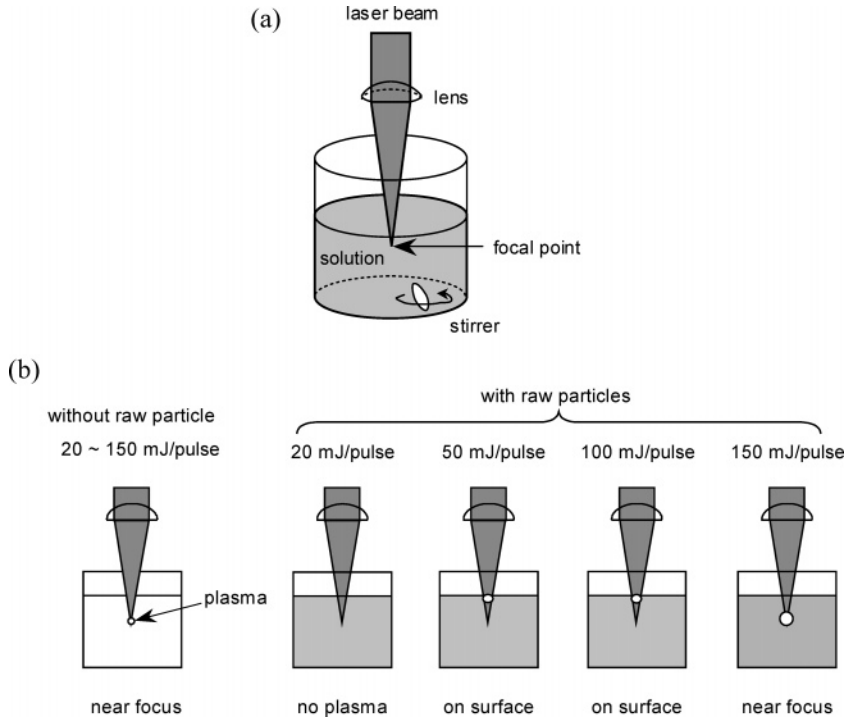

Figure 1. (a) Schematic configuration of laser irradiation of raw ITO nanoparticles in water and (b) position of plasma emission generated by laser irradiation with various laser energies for the colloidal solutions with and without raw ITO nanoparticles.

(FE-SEM, Hitachi S-4800) and a transmission electron microscope (TEM, JEOL JEM-2000-FX). An energy-dispersive X-ray (EDX) spectroscopy system equipped with a TEM was used to analyze the chemical composition of the nanoparticles.

3. Results and Discussions

3.1. Physical Appearance of Plasma during Laser Irradiation. Optical breakdown of water takes place easily when irradiated by a pulsed and focused laser beam.[15] To confirm that laser irradiation would cause breakdown in our experiments, we first conducted a control experiment in which only deionized water was irradiated without the raw ITO nanoparticles. Sound generated by the breakdown with a higher sound intensity level was detected at all laser energies when intense photoemission from the plasma was observed. The plasma emission was observed near the focal point below the water level over the laser safety glasses (Figure 1b). The sound is generally caused by the collapse of a vaporized cavitation bubble in liquid.[15,16] This result demonstrated that the breakdown of water occurred even at the lowest laser energy of 20 mJ/pulse.

When the raw ITO nanoparticles in water were irradiated at 50 mJ/pulse and above, sound of the breakdown was detected. The position of the plasma generated by laser irradiation with the various energies of the raw ITO nanoparticles in water is illustrated in Figure 1b. The bright spark of the plasma plume was not evident at 20 mJ/pulse. However, plasma was found on the surface of the solution at energies of 50 and 100 mJ/pulse. Laser irradiation of 150 mJ/pulse produced a larger plasma emission near the focal point below the water level. The variation of the geometrical position of the plasma during laser irradiation implied a mechanism of the breakdown.[16,17] The irradiated laser beam induced a strong electric dipole around the nanoparticle under quasi-electrostatic approximation because the particle was much smaller than the wavelength of the irradiated laser in this experiment. The electric field of the dipole caused an electron avalanche near the nanoparticles and a breakdown of water; as a result, the threshold laser energy of the breakdown became much lower than that of pure water without nanoparticles. Therefore, a breakdown of water with the nanoparticles seemed to occur in front of the focal point at 50 and 100 mJ/pulse. The reason that we could observe neither plasma emission nor sound of the breakdown at 20 mJ/pulse could be that the breakdown region was very small due to laser energy decay by the dispersed nanoparticles. In contrast, laser irradiation at 150 mJ/pulse possibly induced the breakdown of water in the larger region between the liquid surface and the focal point. In this case, we presumably observed the brightest plasma emission near the focal point. Thus, the breakdown of water in a colloidal solution was expected to play an important role in the fragmentation of particles.

TABLE 1: Zeta Potential, Average Size, and Optical Band Gap E_{opt} of the Raw ITO Nanoparticles and the Irradiated Nanoparticles at Various Laser Energies

	zeta potential (mV)	average size (nm)		E_{opt} (eV)
		secondary particles	primary particles	
before irradiation	−21.1	902	30.6	3.82
irradiated at 20 mJ/pulse	−20.3	810	14.5	3.91
50 mJ/pulse	28.6	197	7.7	4.01
100 mJ/pulse	29.4	191	5.2	4.08
150 mJ/pulse	37.0	188	3.0	4.15
150 mJ/pulse (posttreated with surfactant)				3.91

3.2. Aggregation of Nanoparticles. The isoelectric point of ITO nanoparticles in water has been reported to be 6.0,[18] and the zeta potential was drastically changed around this pH value. In this study, the pH value of the colloidal solution before laser irradiation was 7.3, and the zeta potential was abruptly changed from a negative to a positive value above 20 mJ/pulse (Table 1). This result may imply that the water breakdown caused the generation of protons and oxygen gas by the dissociation of water molecules, and the pH value dropped to less than 6.0 due to the laser irradiation.

The average size of secondary particles obtained by the dynamic light-scattering method is presented in Table 1. A larger

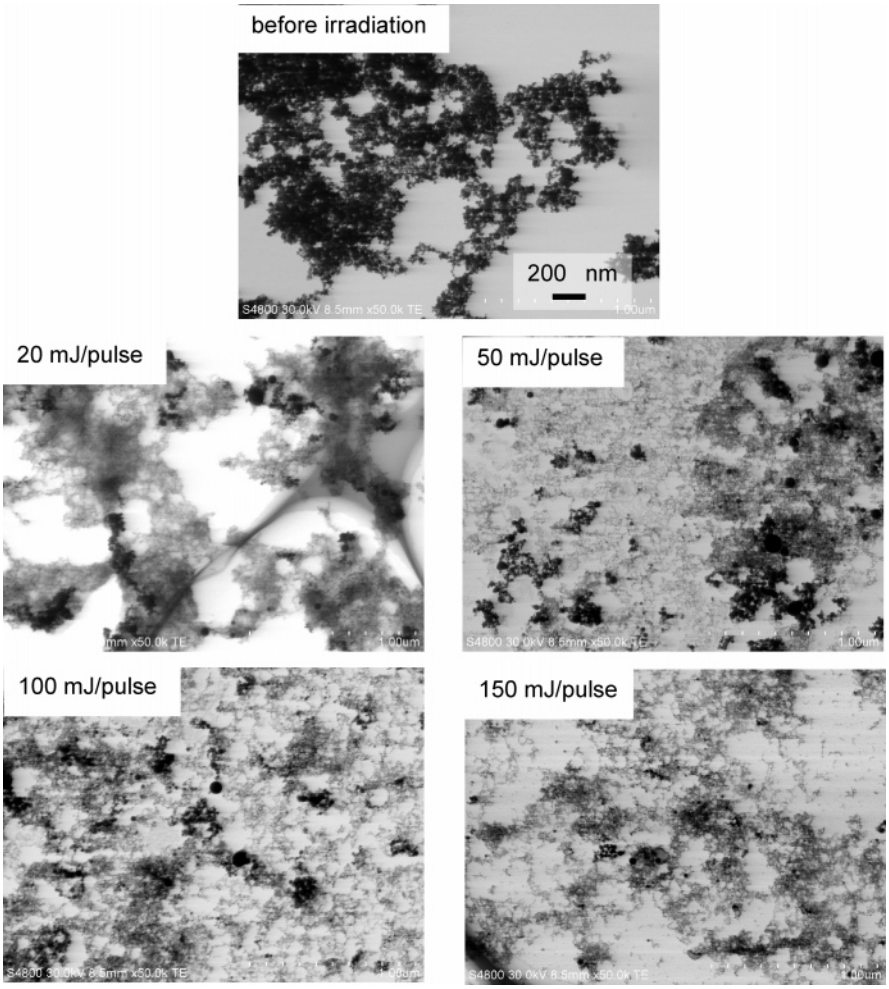

Figure 2. Scanning transmission electron microscopic images by FE-SEM of the raw ITO nanoparticles and the irradiated nanoparticles at various laser energies.

average size of secondary particles was observed for raw ITO nanoparticles and irradiated nanoparticles at 20 mJ/pulse. The ITO nanoparticles strongly aggregated due to a small electrostatic repulsive force between them because the absolute value of the zeta potential was small. Figure 2 depicts scanning transmission electron images by FE-SEM of the raw ITO nanoparticles and irradiated nanoparticles. The strong aggregation and larger interspace between aggregated nanoparticles were confirmed by FE-SEM observation of the raw nanoparticles and irradiated nanoparticles at 20 mJ/pulse.

3.3. Crystal Structure. The crystal structure of Sn-doped In_2O_3 (ITO) is the same as that of In_2O_3 because Sn ions are substituted for In ion sites in the In_2O_3 lattice.[19] The crystal structure of the raw nanoparticles was found to be cubic In_2O_3 (JCPDS Card No. 06-0416) by XRD. In contrast, we could not definitively assign the crystal structure of the irradiated nanoparticles because the precipitate for XRD measurement included both raw nanoparticles and irradiated nanoparticles and analytical separation of XRD peaks was difficult. However, we overcome this problem by analysis of selected area electron diffraction.

Figure 3 presents the TEM images and selected area electron diffraction patterns of raw nanoparticles and the irradiated nanoparticles at various laser energies. The electron diffraction patterns of the raw nanoparticles agreed with the pattern of the cubic In_2O_3, supporting the XRD result. The Debye ring of the irradiated nanoparticles at 20 mJ/pulse indicated that the crystal structure of the irradiated nanoparticles was also the cubic In_2O_3. However, a vague halo was observed for irradiated nanoparticles above 20 mJ/pulse. This halo indicated particle size decrease by fragmentation and degradation of crystallinity in the smaller particles fabricated at much higher laser energy, where ablation of nanoparticles also took place with the breakdown of water. The average size of primary particles determined from the TEM images decreased with increasing laser energy as (Table 1). The ITO nanoparticles were obviously fragmented even by the lowest laser energy of 20 mJ/pulse, although no plasma emission or sound of the breakdown was observed during laser irradiation at this laser energy. A localized breakdown of water, however, did occur on the surface or near the focal point, and the cavitation and shock wave created by the breakdown mechanically fragmented the raw nanoparticles. Fragmentation by the breakdown of water proceeded with increasing laser energy. In particular, the fragmented nanoparticles at 150 mJ/pulse exhibited an extremely small average size (3.0 nm) of primary particles. The Sn/In ratio of the fragmented nanoparticles at 100 mJ/pulse was found to be 1:9 by the EDX measurement in the TEM; thus, the Sn/In ratio did not change during laser irradiation. Consequently, the fragmented nanoparticles were supposed to be ITO nanoparticles, although the oxygen stoichiometry in ITO nanoparticles might be changed from that of the raw ITO nanoparticles.

3.4. Optical Transmittance Spectrum. The ITO is transparent in the visible region because the band gap is about 3.90 eV (318 nm).[20] Thus, Mie scattering affected the transmittance spectrum of the colloidal solution of the ITO nanoparticles in

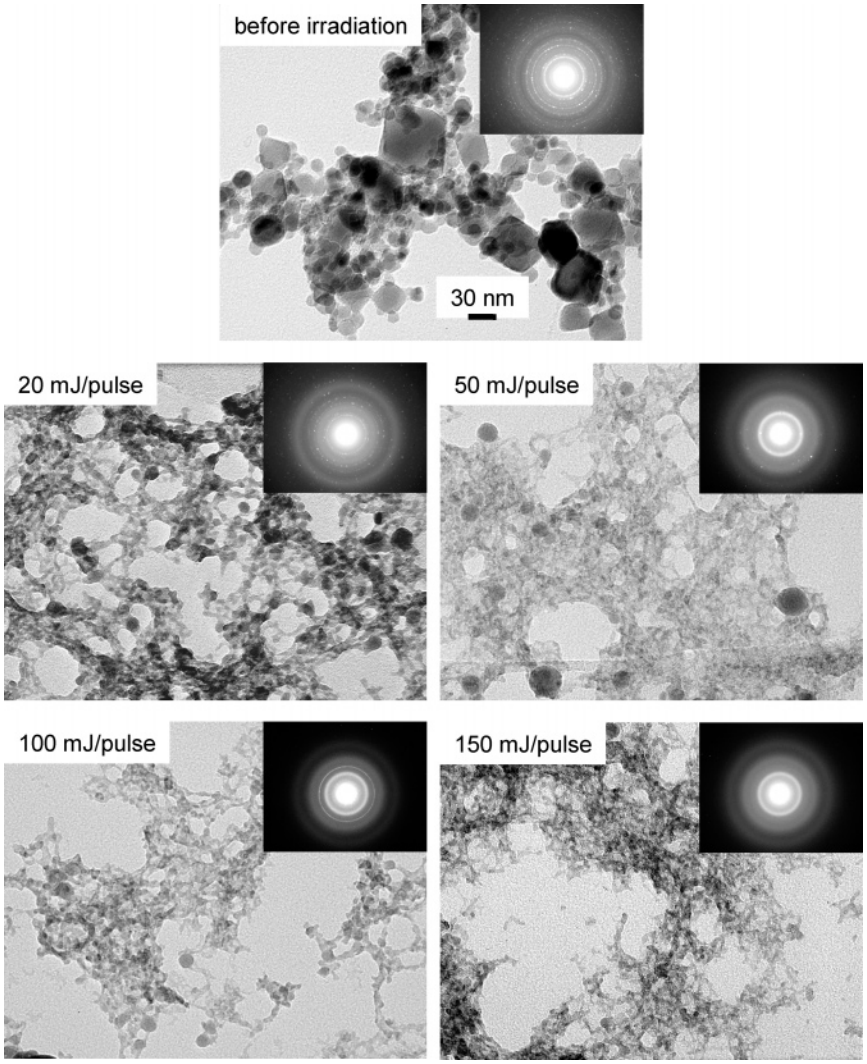

Figure 3. Transmission electron microscopy images and selected area electron diffraction patterns of the raw ITO nanoparticles and the irradiated nanoparticles at the various laser energies.

the visible region because the secondary particle size of the aggregated nanoparticles was comparable to the wavelength of visible light. Figure 4a shows the transmittance spectrum in the UV−vis region of the colloidal solutions of raw ITO nanoparticles and irradiated nanoparticles at all laser energies. Transmittance in the visible region slightly increased with increasing laser energy, implying that Mie scattering intensity by aggregated nanoparticles decreased because the secondary particle size decreased with increasing laser energy (Table 1). In contrast, Rayleigh scattering is strongly pronounced when particle size is much smaller than one-tenth of the incident light wavelength, and the scattering intensity is inversely proportional to the fourth power of the wavelength. At 150 mJ/pulse, the average size of the primary particles was 3.0 nm, which was much smaller than one-tenth of the wavelength of the shorter UV region (200−250 nm). Therefore, the transmittance in this region rapidly decreased with decreasing wavelength due to the Rayleigh scattering effect. Thus, the fragmented nanoparticles at higher laser energy were more suitable for the transparent coating material of a UV shield.

The absorption coefficient α was determined from transmittance using the Lambert−Beer law. Figure 4b depicts a variation of the square of the absorption coefficient α^2 with photon energy. This figure clearly indicates that the absorption edge shifted to larger photon energy with increasing laser energy. The optical band gap E_{opt} could be estimated by extrapolating the linear portion of α^2−photon energy curves.[21] Since the absorption spectra might include not only the light absorption of the nanoparticles but also the effect of Mie scattering, we made only a relative comparison using the obtained E_{opt}. However, the obtained E_{opt} (3.82 eV) of the raw ITO nanoparticles in solution was reasonable because the diffuse reflectance spectrum measurement of the powder of raw ITO nanoparticles showed E_{opt} of 3.90 eV, which should reflect the absorption of the nanoparticles without the effect of Mie scattering. The E_{opt} increased with the decreasing average size of primary particles (Figure 5). Two possible reasons for the increase in E_{opt} are suggested. (i) Quantum size effects may appear for the fragmented nanoparticles. The quantum size effects of ITO nanoparticles have been previously reported to be observed at 50 nm or smaller.[22] In our experiments, the quantum size effects may have appeared because the fragmented nanoparticles were much smaller than 50 nm. (ii) The Burstein−Moss effect might occur due to the increase in carrier concentration.[23] The carrier origin of ITO is doped Sn and oxygen vacancies.[24] Generally, when the Sn/In ratio is 1:9, ITO nanoparticles have the largest carrier concentration and the highest electric conductivity.[25] Since the Sn/In ratio of both the raw ITO nanoparticles and the fragmented nanoparticles at 100 mJ/pulse were confirmed to be 1:9, the reason for the carrier increase was supposed to be

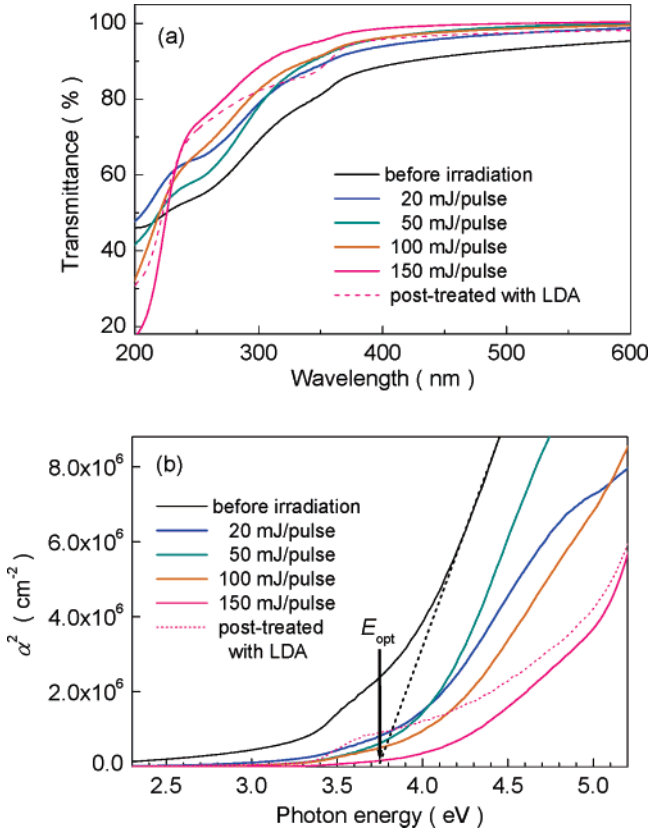

Figure 4. (a) Optical transmittance spectra of the colloidal solutions of the raw ITO nanoparticles and the irradiated nanoparticles at various laser energies. (b) Variation of the square of the absorption coefficient α^2 of the solutions with the photon energy. The nanoparticles irradiated at 150 mJ/pulse were posttreated using the surfactant LDA for comparison.

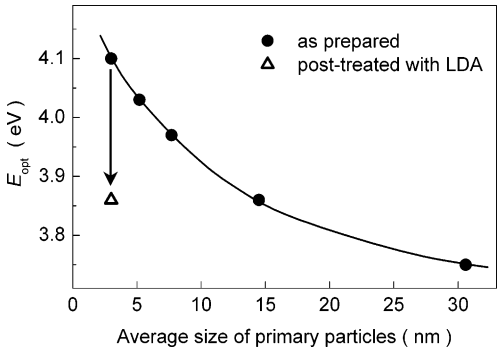

Figure 5. Relationship between the average size of primary particles and optical band gap E_{opt} of the ITO nanoparticles. The ITO nanoparticles with the smallest particle size were posttreated with the surfactant LDA.

the increase of oxygen vacancies produced by the laser fragmentation of ITO nanoparticles. Smaller nanoparticles of metal oxide probably had lattice defect of oxygen vacancies on the surface. The surface defects of oxygen vacancies can be passivated by the oxygen of surfactant molecules in an aqueous solution as described in our previous experiments on ZnO nanoparticles.[8]

Therefore, we carried out the surfactant treatment using an aqueous solution of lauryl dimethylaminoacetic acid betaine (LDA; $CH_3(CH_2)_{11}N(CH_3)_2CH_2COO$) at a concentration of 2.5×10^{-4} mol/L, which has been found to be an optimal condition for the passivation of surface defects, for the fragmented nanoparticles at 150 mJ/pulse. The transmittance spectrum and

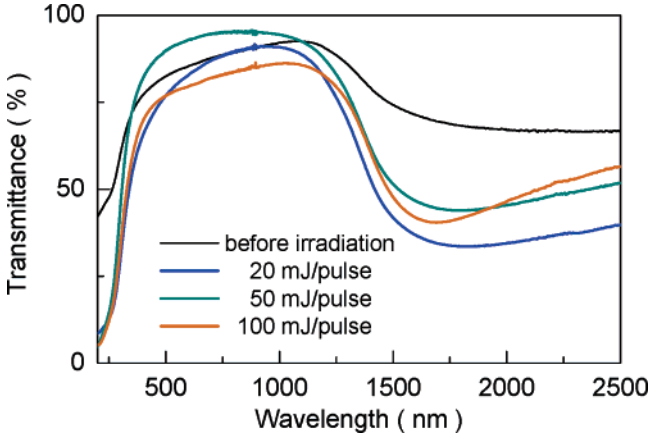

Figure 6. Optical transmittance spectra in the UV−vis−IR region of the films of the raw ITO nanoparticles and the irradiated nanoparticles at various laser energies.

α^2−photon energy curve of the solution after the surfactant treatment are plotted in Figures 4a and 4b. The surfactant treatment decreased E_{opt} (Figure 5), indicating that the carrier concentration was decreased by the passivation of oxygen vacancies on the surfaces of the fragmented ITO nanoparticles. Therefore, the reason for the E_{opt} increase was probably oxygen vacancies generated by laser-induced fragmentation.

The transmittance in the UV−vis−IR region was measured for dried precipitate films of the raw ITO nanoparticles and the irradiated nanoparticles. The precipitated film could not be prepared for the nanoparticles irradiated at 150 mJ/pulse due to the good dispersion of the irradiated nanoparticles in the solution. Thus, Figure 6 shows the optical transmittance spectra in UV−vis−IR of the films of the raw ITO nanoparticles and the irradiated nanoparticles, except for those irradiated at 150 mJ/pulse. The films of the irradiated nanoparticles exhibited higher transmittances in the visible region and lower transmittances in the UV and IR regions than raw nanoparticle films. A critical wavelength from transmission to reflection of IR was determined as a plasma frequency using the Drude theory.[26,27] The critical wavelength was inversely proportional to the square root of the carrier concentration. The significant transmittance decrease in the IR region by laser irradiation may be attributed to a shift of the critical wavelength to a shorter wavelength because of the increased carrier concentration. This result supports the E_{opt} increase by the Burstein−Moss effect. A possible reason for the lower transmittance in the UV region for the films of the irradiated nanoparticles could be that the irradiated nanoparticles uniformly covered the glass substrate of the films without interspaces between the aggregated nanoparticles, due to being well dispersed, and the incident light was effectively absorbed by the films. These results suggest that the laser-induced fragmented ITO nanoparticles are promising for UV and IR shielding materials.

4. Conclusion

Laser irradiation of ITO nanoparticles was carried out in water using various laser energies to fabricate smaller nanoparticles by laser-induced fragmentation. We investigated the influence of laser energy on the particle size and the transmittance spectrum of fragmented nanoparticles. The fragmentation of nanoparticles by water breakdown proceeded with increasing laser energy. The average size of the fragmented nanoparticles decreased with increasing laser energy. The fragmented nanoparticles showed high transmittance in the visible region and

lowered transmittance in the UV and IR regions. The optical band gap of the fragmented nanoparticles increased with decreasing average particle size. This result was possibly caused by the Burstein−Moss effect, due to the increasing concentration of the carriers generated by the surface defects of the oxygen vacancies. These defects might be generated on the particle surface when raw ITO nanoparticles were mechanically fragmented by the shock wave and cavitation effects of the water breakdown.

Acknowledgment. This study was partially supported by Industrial Technology Research Grant Program 2005 from the New Energy and Industrial Technology Development Organization of Japan.

References and Notes

(1) Simakin, A. V.; Voronov, V. V.; Shafeev, G. A.; Brayner, R.; Bozon-Verduraz, F. *Chem. Phys. Lett.* **2001**, *348*, 182.
(2) Mafuné, F.; Kondow, T. *Chem. Phys. Lett*. **2003**, *372*, 199.
(3) Mafuné, F.; Kondow, T. *Chem. Phys. Lett.* **2004**, *383*, 343.
(4) Wang, J. B.; Zhang, C. Y.; Zhong, X. L.; Yang, G. W. *Chem. Phys. Lett.* **2002**, *361*, 86.
(5) Chen, Y. H.; Yeh, C. S. *Colloids Surf., A* **2002**, *197*, 133.
(6) Sasaki, T.; Liang, C. H.; Shimizu, Y.; Koshizaki, N. *Appl. Phys. A* **2004**, *79*, 1489.
(7) Sakka, T.; Saito, K.; Ogata, Y. H. *Appl. Surf. Sci.* **2002**, *197*, 246.
(8) Usui, H.; Shimizu, Y.; Sasaki, T.; Koshizaki, N. *J. Phys. Chem. B* **2004**, *109*, 120.
(9) Usui, H.; Sasaki, T.; Koshizaki, N. *Chem. Lett.* **2005**, *34*, 700.
(10) Nichols, W. T.; Kodaira, T.; Sasaki, Y.; Shimizu, Y.; Sasaki, T.; Koshizaki, N. *J. Phys. Chem. B* **2006**, *110*, 83.
(11) Tsuji, T.; Higuchi, T.; Tsuji, M. *Chem. Lett.* **2005**, *34*, 476.
(12) Kim, K. Y.; Park, S. B. *Mater. Chem. Phys.* **2004**, *86*, 210.
(13) Ederth, J.; Johnsson, P.; Niklasson, G. A.; Hoel, A.; Hultåker, A.; Heszler, P.; Granqvist, C. G.; Doorn, A. R. V.; Jongerius, M. J. *Phys. Rev. B* **2003**, *68*, 155410.
(14) Song, J. E.; Lee, D. K.; Kim, H. W.; Kim, Y. I.; Kang, Y. S. *Colloids Surf., A* **2005**, *257*, 539.
(15) Vogel, A.; Noack, J.; Nahen, K.; Theisen, D.; Busch, S.; Parlitz, U.; Hammer, D. X.; Noojin, G. D.; Rockwell, B. A.; Birngruber, R. *Appl. Phys. B* **1999**, *68*, 271.
(16) Sylvestre, J.-P.; Kabashin, A. V.; Sacher, E.; Meunier, M. *Appl. Phys. A* **2005**, *80*, 753.
(17) Besner, S.; Degorce, J.-Y.; Kabashin, A. V.; Meunier, M. *Appl. Surf. Sci.* **2005**, *247*, 163.
(18) Sun, J.; Velamakannni, B. V.; Gerberich, W. W.; Francis, L. F. *J. Colloid Interface Sci.* **2004**, *280*, 387.
(19) Hamberg, I.; Granqvist, C. G. *J. Appl. Phys.* **1986**, *60*, 123.
(20) Maki, K.; Komiya, N.; Suzuki, A. *Thin Solid Films* **2003**, *445*, 224.
(21) Zhou, Z. B.; Cui, R. Q.; Pang, Q. J.; Wang, Y. D.; Meng, F. Y.; Sun, T. T.; Ding, Z. M.; Yu, X. B. *Appl. Surf. Sci.* **2001**, *172*, 245.
(22) Cui, H. N.; Teixeira, V.; Monteiro, A. *Vacuum* **2002**, *62*, 589.
(23) Ramaiah, K. S.; Raja, V. S.; Bhatnagar, A. K.; Tomlinson, R. D.; Pilkington, R. D.; Hill, A. E.; S. J. Chang,; Su, Y. K.; Juang, F. S. *Semicond. Sci. Technol.* **2000**, *15*, 676.
(24) Ray, S.; Banerjee, R.; Basu, N.; Batabyal, A. K.; Barua, A. K. *J. Appl. Phys.* **1983**, *54*, 3497.
(25) Lee, D. H.; Vuong, K. D.; Williams, J. A. A.; Fagan, J.; Condrate, R. A.; Wang Sr., X.; Wang, W. *J. Mater. Res.* **1996**, *11*, 895.
(26) Bender, M.; Seelig, W.; Daube, C.; Frankenberger, H.; Ocker, B.; Stollenwerk, J. *Thin Solid Films* **1982**, *326*, 72.
(27) Lee, H.-C. *Appl. Surf. Sci.* **2006**, *252*, 2647.